6th International Workshop on Microsystems

Alexander Campus, International Hellenic University, 15 December 2021

Workshop Proceedings

Introduction

This workshop brings together research and development from a large spectrum of science and engineering fields related to the implementation of microsystems in the new era of distributed information technologies. As cloud computing services and smart portable systems are becoming ubiquitous and more advanced, new possibilities for interdisciplinary research emerge. The microsystems that comprise the so-called internet of things will encompass a wide range of technologies including new energy sources, energy and information electronics, sensor systems, smart and energy efficient control and computing, telecommunications and networking, and also nanotechnology and micro-electro-mechanical systems. Continuing five successful workshops between 2016 and 2020, the 6th International Workshop on Microsystems aims at bringing together related research and development advancements from the academic community and the industry. Scientific topics include but are not limited to:

- Energy microsystems
- Sensors and sensor electronics
- Embedded systems
- Integrated Circuits and Systems
- Industrial automation and control
- Microelectronics and nanoelectronics
- Micro-electro-mechanical systems
- Computing for microsystems

Michail E. Kiziroglou
m.kiziroglou@ihu.gr

Venue

Lecture Theater, Automation and Informatics Building
Sindos Campus, ATEI Thessaloniki, Greece

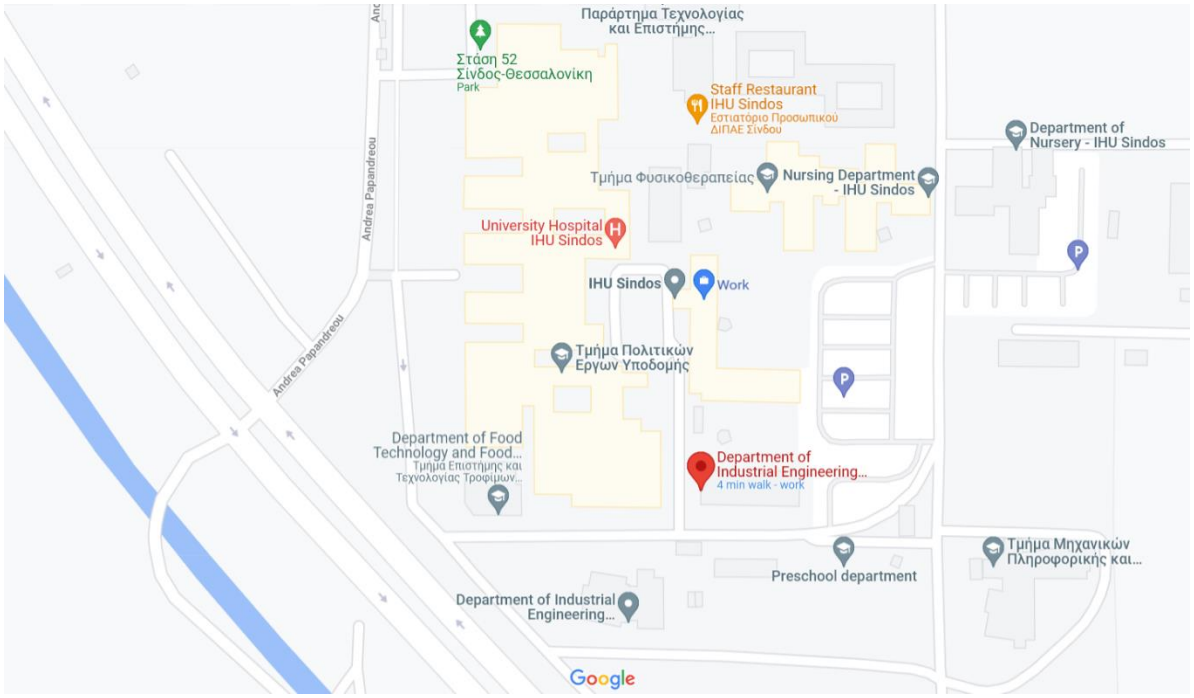

Date

Wednesday, 15th of December, 2021

Organizer

Michail E. Kiziroglou

Session Chair

Dr. Dimitris Triantafyllidis, Industrial Eng. & Management, IHU

Technical Programme Committee

Alexandros Astaras
Dimitrios Bechtsis
Michail E. Kiziroglou
Simira Papadopoulou
Fotis Stergiopoulos
Dimitris Triantafyllidis
Kostas Siozios
Apostolos Tsagaris
Christos Yfoulis
A. Hatzopoulos

Organization and Technical Support

Ourania Banti, Maria Michailidou and Maria Pagkrakioti

List of Authors

No	First Name	Last Name	Affiliation
1	Ourania	Banti	IHU
2	Dimitrios	Bechtsis	IHU
3	Aristotelis	Boukogiannis	IHU
4	Vasileios	Fountas	AUTH
5	Efstratios	Gkagkanis	IHU
6	Alkis	Hatzopoulos	AUTH
7	Argyrios	Hatzopoulos	IHU, Dep. Information & Electr. Syst. Engineering
8	Konstantinos	Karakostas	Echovista GmbH, United Kingdom
9	Michail E.	Kiziroglou	IHU
10	Georgios	Kokkas	IHU
11	K.	Kostopoulos	IHU
12	Dimitrios	Makarikas	IHU
13	Maria	Michailidou	IHU
14	M.	Mytilinaios	IHU
15	Dimitrios K.	Papakostas	IHU, Dep. Information & Electr. Syst. Engineering
16	Fotis	Stergiopoulos	IHU
17	Alexandros	Styliadis-Heinz	IHU
18	Dimitris	Triantafyllidis	IHU
19	Dimitrios	Tsoukalas	NTUA
20	Vassileios	Vassios	IHU, Dep. Information & Electr. Syst. Engineering

Programme

08:45-09:00: Registration

Please check-in or register at the front desk.

09:00-09:15: Welcome and introduction

09:15-10:45: First Oral Session (Session Chair: Dr. D. Triantafyllidis, IHU)

09:15 – 10:00: Nanoparticle based sensors. *Prof. Dimitris Tsoukalas, Dept. of Physics, National Technical University of Athens* 21WOM-01 (keynote, invited).

10:00: Design and Construction of an Automated Milling Machine for producing PCBs. *M. Mytilinaios and D. Triantafyllidis*, 21WOM-02.

10:15: A python software tool for 2D and 3D image processing, *A. Boukogiannis and D. Bechtsis*, 21WOM-03.

10:30: Design Framework of a Decision Support System used in a Canning Industry, *G. Kokkas, A. Styliadis-Heinz, F. Stergiopoulos and D. Bechtsis*, 21WOM-04.

10:45-11:15: Coffee Break and Poster Session

Fabrication and Development of an Optical Biomedical Sensor, *O. Banti, M. Michailidou, E. Gkagkanis, K. Karakostas and M. E. Kiziroglou*, 21WOM-05.

11:15-12:00: Second Oral Session (Session Chair: Dr. D. Triantafyllidis, IHU)

11:15: A Novel Approach on Fault Detection of Analog and Mixed Signal Circuits by monitoring the fluctuation of the Supply Current, *V. D. Vassios, A.T. Hatzopoulos and D. K. Papakostas*, 21WOM-06.

11:30: Rectification and boosting circuit for acoustic power transfer, *V. Fountas, D. Makarikas, M. E. Kiziroglou, K. Karakostas and A. Chatzopoulos*, 21WOM-07.

11:45: Automation of a Washing Machine: An Open-Source Approach, *K. Kostopoulos and D. Triantafyllidis*, 21WOM-08.

12:00-12:15: Best Paper Award by Ioannidis Electronics. Concluding remarks.

WORKSHOP ABSTRACTS

Nanoparticle based sensors

Dimitris Tsoukalas
Dept. of Physics, National Technical University of Athens

The expansion of the Internet of Things will increasingly require the use of a huge number of sensing devices for measuring environmental parameters or for structural health monitoring of buildings and large infrasrtucture while is is also expected to be used even for human body parameters surveillance. On the other hand the field of nanotechnology that has already two decades of scientific life, has made remarkable progress related to the bottom-up controlled fabrication of nanostructures. In this presentation we shall discuss the application of a nanotechnology approach for the fabrication of nanoparticle based sensors together with their applications (fig. 1). More particulraly we shall empasize on physical sensors that measure strain or pressure which are made on rigid, flexible or even strechable substrates followed by a dicussion of chemical sensors and biosensors to monitor environmental parameters [1.-3].

Fig. 1. A flexible strain nanoparticle sensor in the middle with a number of potential application examples.

References

[1] E. Aslanidis, E. Skotadis, D.Tsoukalas Nanoscale 13 (5), 3263-3274 (2021)
[2] E. Skotadis et al. Computers and electronics in agriculture 178, 105759 (2020)
[3] L. Madianos et al. Biosensors and Bioelectronics 101, 268-274 (2018)

Design and Construction of an Automated Milling Machine for producing PCBs

M. Mytilinaios and D. Triantafyllidis+

International Hellenic University / Department of Industrial Engineering & Management
P.O. Box 141, 57 400 Sindos, Thessaloniki, Greece

+ Corresponding author: drdimitri@autom.teithe.gr

***Abstract* — The present paper presents the design and construction of an automated milling machine suitable for engraving electronic circuits also known as "Printed Circuits" on bakelite single sided copper boards (PCBs). The topics that are included are the design considerations, the assembly of the hardware and the setting up of the machine. The required steps for producing an exemplary PCB are also presented.**

Keywords — CNC, Milling Machine, PCB.

I. INTRODUCTION

Computer Numerical Control also known as CNC machines are machines that can process a piece of raw material (metal, wood, plastic acrylic, etc.) into a component of another machine or a complete product as it is. This is accomplished with a spindle that rotates in a specific number of RPMs that are chosen by the user. A specific end mill cutter must be installed depending on the material and the spindle will move in a 3-axis system (X, Y, Z) accurately with stepper motors. By rotating and passing through the material, it carves it, giving it the desired geometry. Creating a 3D model of the machine is the first step, as well as the calculation and the selection of the stepper motors and the motherboard with the microprocessor. In order to prevent any damage to the machine, preventive measures such as terminal switches must be added to ensure the safety of the machine and the machinist. After installing the hardware components in a correct electrical and mechanical manner, the user must program and initialize the motherboard. The next step is the creation of a file which contains all the information for the CNC procedure. Lastly, the proper placement of the PCB on the workspace of the CNC is crucial in order to secure a stable and uniform result. The present paper presents the design criteria, the assembly, and the initial parameters of the machine, as well as the PCB design stages and an example of a produced PCB.

II. DESIGN CRITERIA

The main factors that must be taken into consideration are firstly the material that will be processed and the size of the workspace in order to build the machine. In this aspect, the following must be decided:

- Size of mechanical parts: By calculating these, the size of the clear workspace can be decided as well as the stability of the structure of the machine.
- Type of end mill cutters: Depending on the material that is being processed, and the type of process, a specific end mill cutter must be chosen for the desirable result. Some applications require more than one type of cutters and after each running process the cutters have to be switched.
- Power of spindle: The max torque and RPMs are the most important parameters in a spindle because they determine the capabilities of the spindle. It is very helpful to have a strong machine but sometimes the excessive force and speed might ruin the material, so it is crucial to be aware of the process details of each material.
- Power of stepper motors: The higher the current that flows to the motor, the higher the torque and precision it possesses. Therefore, for heavy loads bigger stepper motors are preferred. In the present project a medium size stepper motor will ensure stability, accuracy and low temperatures during the working process.
- Type of motherboard and drivers: To obtain the control and the proper movement of the 3-axis system the motherboard must be initially programmed. For the present project the motors have a pre-installed driver board on them. Except for the movement control these boards are designed to give feedback in a closed loop to the motherboard in order to correct any lost steps which would translate into wrong movement.
- Software: Lastly, in order to translate a 3D model of a PCB into machine movements, a file must be created that contains all the information about the PCB in order for the machine to execute the exact procedure steps.

To simplify the design criteria process a readily available CNC kit from BigTreeTech [1], including the required motherboard, stepper motors, and closed loop drivers has been selected, thus avoiding possible incompatibilities. The motherboard utilizes an Arduino nano V3.0 ATMEGA328P (DCCduino Nano) microcontroller (Fig. 1).

III. ASSEMBLY

The assembly of the mechanical parts took place very carefully, with high precision, in order to ensure a smooth operation of the machine with high accuracy. The parts were customized and cut for a workspace that can fit a large range of sizes of PCBs. Along with the CNC machine, a control box has been designed and installed for a user- friendly interface. A photo of the assembly follows in Fig. 2.

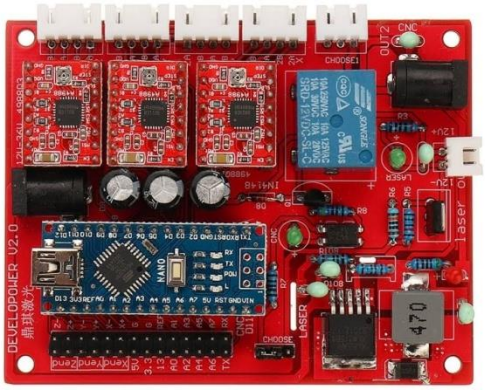

Figure 1: The motherboard with the Arduino nano V3.0 ATMEGA328P. On the top side the three motor drivers can be seen.

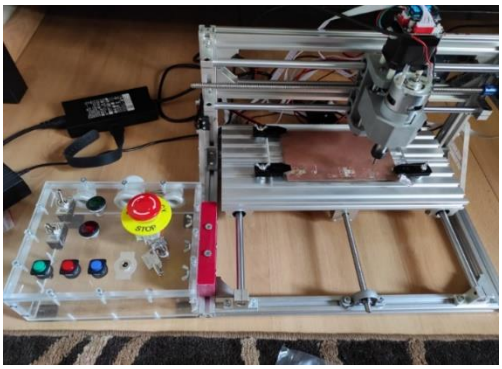

Figure 2: Assembly of mechanical and electric parts of the CNC machine.

IV. Initial Parameters

The parameters that are required for the proper function of the machine have to be programmed into the machine. The programming is being done via serial port. The firmware that was used for the present project is called GRBL [2, 3]. It contains numerous variables which determine parameters such as the speed of movement, the acceleration, the deceleration, the coordinates of starting, stopping, and parking of the spindle, etc. Additionally, a software responsible for the safety of the machine and the user, called Termite [4] has been used. Termite monitors the installed terminal switches, causing an immediate shut down when required, preventing major accidents.

V. PCB Design Steps

There are several levels of information and steps that are required to design and manufacture a PCB. The first step is to create a Gerber file, a type of file that contains information such as the size and the frame of the PCB, the number and size of the holes, the geometry of the product etc. A student version of the Altium software [5] has been used in order to describe all the aspects of the PCB (Fig. 3). Altium offers a 3D representation of the PCB as well as a search library with existing components from the electronic market all around the world. When the designing process concludes, Altium exports the 3D file into a Gerber file.

The second step starts with the FlatCAM software [6], which accepts Gerber files, and modifies the geometrical information of the PCB into machine commands (G-Code) including various processes which may need multiple passes, or tool changes.

The third step requires a software called Candle [7], a program that connects to the CNC machine via serial port and can accept G-Code commands or direct commands from the user. Candle is additionally used to probe the height of the PCB at various points in order to create a height map, which is used to adjust for required corrections of the cutting depth.

Figure 3. PCB Design in Altium (Cutout, Engrave, Drill).

With the exception of Altium, all other special software required for this project was freely available, under various license agreements, requirements or limitations.

VI. Production Process & Results

For the process to start, the blank PCB is firmly hold in position with the help of acrylic plates. This is to prevent the collision of the end mill with the workspace and to provide adequate toughness and stiffness to avoid bending of the PCB. Double sided tape is added to the back of the PCB to ensure zero movement. As soon as the process begins the user must wear safety glasses and maintain a respectful distance from the machine, placing the hand on the emergency stop button in case of misjudged movement of the spindle. An example of the resulting product follows in Fig.4

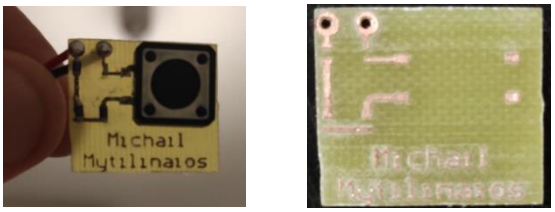

Figure 4. Resulting product.

VII. Conclusions and Future Work

Despite the time-consuming process, the machine satisfies the user with its end results. The cost to manufacture the prototype CNC machine was about 500 €, which may be considered quite high, but nevertheless it allows the user to create PCBs independently without having to outsource them, thus avoiding minimum number of copies requirements as well as shipping times. Further improvements can be made such as implementing a larger spindle motor or designing an aluminum motor base for minimizing vibrations.

References

[1] https://www.biqu.equipment/
[2] GRBL:https://diymachining.com/grbl-settings-101-a-how-to-guide/
[3] https://www.cnc.com/grbl-controller/
[4] Termite: https://www.compuphase.com/software_termite.htm
[5] Altium:http://valhalla.altium.com/Learning-Guides/OG0101%20Gerber%20Output%20Options.pdf
[6] FlatCAM: http://flatcam.org/
[7] Candle:https://github.com/Denvi/Candle

A python software tool for 2D and 3D image processing

Aristotelis Boukogiannis and Dimitrios Bechtsis

Industrial Engineering and Management Department, International Hellenic University, Greece

Images and videos captured by RGB and depth cameras could be used in industrial environments for enabling automations. The proposed software tool is developed using the python programming language and open-source libraries (indicatively OpenCV and NumPy) in order to process images and videos in real-time. Hardware and software components are properly combined, and a custom Graphical User Interface (GUI) enables the end user to capture, process and save multimedia content. The RGB camera is capturing images and video streams in the 2D space, while a variety of image processing filters from the above-mentioned libraries process the original files and transform them accordingly (indicatively black and white, gray scale, canny and negative filters). Furthermore, the Kinect v2 depth camera was used in order to capture the 3D environment. The Kinect's libraries were integrated in the software tool in order to create the point cloud environment and visualize it in the GUI. The 3D point cloud is created from 3D voxels, can be saved as a polygon file, and be further processed. The software tool has the sophistication to manipulate the 3D point cloud by parsing the voxels using 3D data structures. Finally, additional features have been included to the software tool for identifying gestures. While a human hand is located in the region of interest the exact gesture is identified and this could trigger a specific action. Indicatively the software tool can identify an open hand and a closed fist ('lasso') to start or stop a specific action. All the developed features could be used in industrial environments either in mobile robots (for navigation and mapping purposes) or even as interfaces for handling machineries (the gesture identification feature could be used to start or stop a production line).

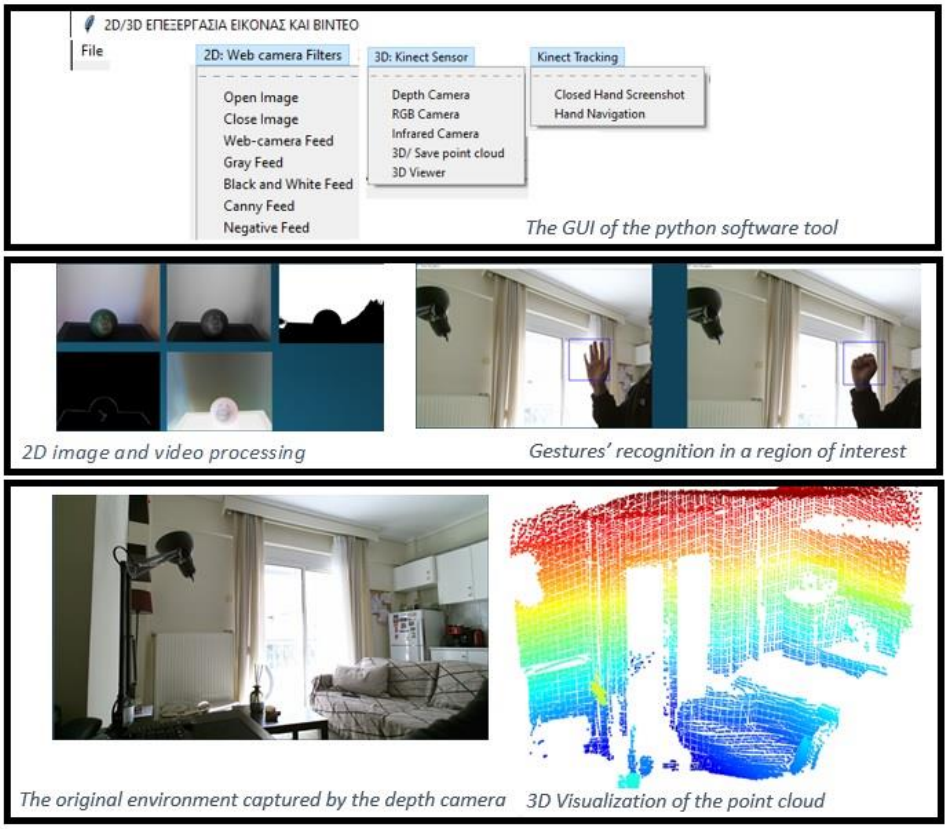

Design Framework of a Decision Support System used in a Canning Industry

Georgios Kokkas(*). Alexandros Styliadis-Heinz, Fotis Stergiopoulos and Dimitrios Bechtsis

International Hellenic University / Department of Industrial Engineering and Management

(*) Corresponding Author, geokokkas87@gmail.com

The manufacturing industry is currently undergoing a digital transformation period with the aim of optimizing and improving the manufacturing process using Information and Communication Technologies (ICT). Decision Support Systems (DSS) play a key role in achieving this goal, both in improving the manufacturing processes by detecting and eliminating bottlenecks and in ensuring maximum uptime through the use of predictive maintenance models.

Our research focuses on the production line of a tin can manufacturing factory where ICT is used to monitor the production processes, improve human-machine interfaces, and use DSS tools. The main objective of the proposed system is to detect and eliminate bottlenecks in the production line. This was achieved by introducing a variety of sensors throughout the production line. Using an OPC Server data were aggregated in a computer and two solutions were examined using the MERN (MySQL-Express-React-Nodejs) technology stack. The first solution is a web-based application (HMI) developed in React, that includes an Express-Nodejs backbone API. This allows production managers and engineers to monitor and interact with the production line in real time from any device that connects to the plant's local area network, while analysts have constant access to real-time and historical production line data. The second solution takes advantage of OPC Server's ability to inherently store production data in a database. Data streams are fed into the Apache Spark software, which processes them and introduces the DSS model, that is then introduced to the web application.

Another added value of the application is that it proposes a framework that reduces the otherwise complicated process of aggregating different sources of manufacturing data and presents them to all the stakeholders using state of the art software tools.

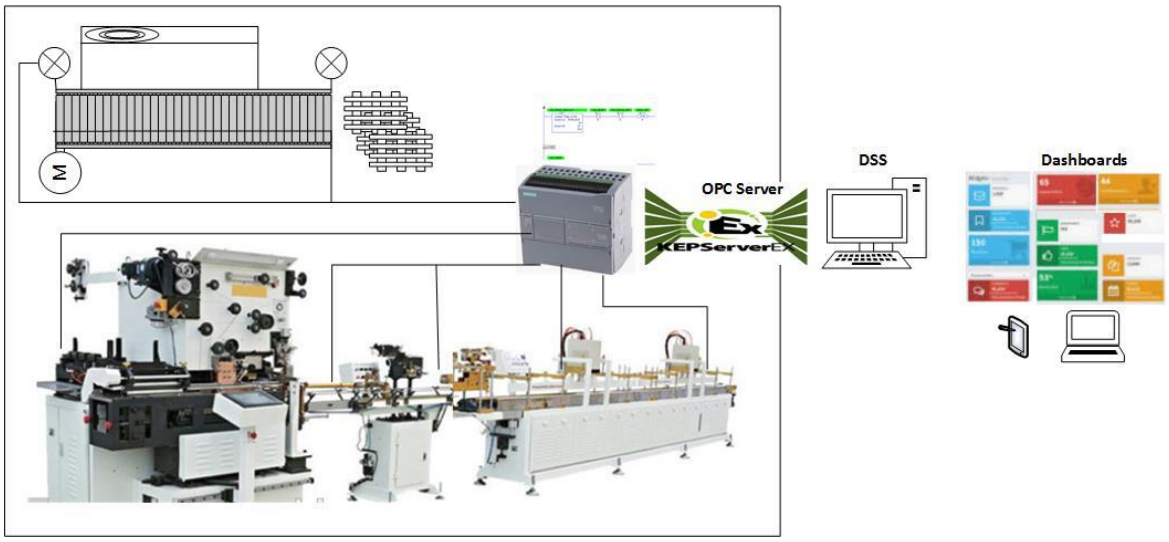

Fabrication and Development of an Optical Biomedical Sensor

O. Banti[†1], M. Michailidou[†1], E. Gkagkanis[1], K. Karakostas[2] ,and M. E. Kiziroglou[1]

Department of Industrial Engineering & Management, International Hellenic University[1], Department of Electronics, Echovista GmbH, United Kingdom[2]

***Abstract*—Portable biomedical devices have proven useful during the COVID-19 pandemic, as devices like optical pulse oximeters and rapid detection tests have been readily available to the public. This paper presents a prototype version of a non-invasive, portable, Mie scattering-based blood quality sensor, developed by the authors for their theses.**

***Index Terms*—biomedical sensors, Mie scattering, circuit board, machine learning, embedded systems, optics, data analysis**

I. Introduction

THIS paper represents the combined efforts of the four authors throughout multiple years. After a proof of concept was submitted by Karakostas et al[2], a prototype of the apparatus was developed by two of the authors. A second, improved version is currently in development, aiming to upgrade the sensor's hardware and optics, implement new features, and improve the data analysis using more advanced algorithms, as well as machine learning.

The apparatus uses a light source and a detector for the detection of Mie scattering in blood cells. Mie scattering describes the behaviour of electromagnetic waves when encountering particles larger or equal to $\frac{1}{10}$ of the wavelength, but is most useful for particles with a diameter comparable to the wavelength. Depending on the wavelength of light and the particle's size and optical properties, a distinct intensity pattern will be identified at different angles of the detector.[1]

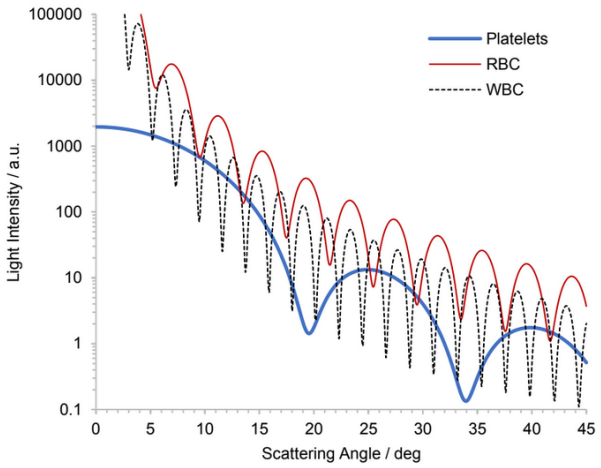

Figure 1: Mie scattering simulation for different types of blood cells, in Mieplot[2][3]

II. Hardware

The prototype was composed of a Beaglebone Black Rev. C microcomputer, a circuit board, a 655nm laser diode, a photodiode array, an RGB LED, a button, and the 3D-printed case. Modifications to the 3D-printed case of the project are crucial to ensure our ability to examine auricular cartilage tissue, as the current housing was designed for in-vitro blood samples in cuvettes and in-vivo finger samples.[1][4]

Moreover, the proper cooling of the Beaglebone Black rev. C,

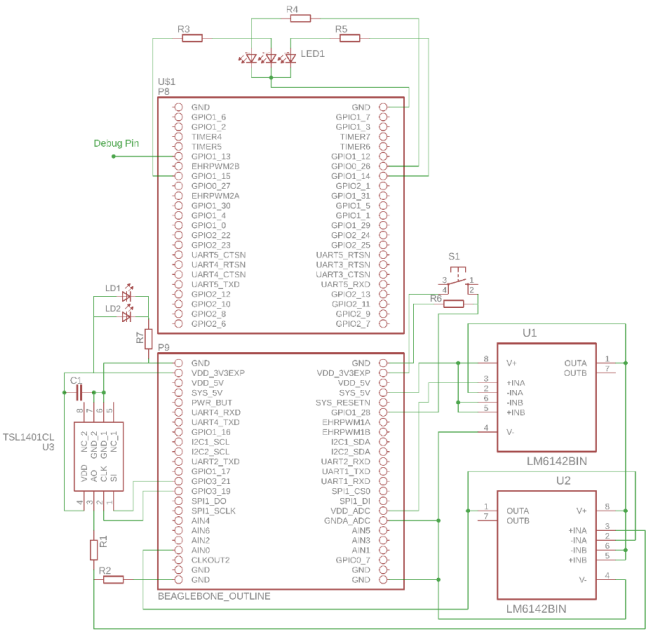

Figure 2: The circuit diagram of the device[4]

which can reach up to 54.6^{o}C, should be taken into account for the longevity of the device. For this purpose, heat sinks and air vents will be added inside the case. Furthermore, the addition of two optical polarizing filters - one in front of the laser beam and one in front of the PDA - were added to the apparatus for noise reduction and polarizing angle experimentation.

III. Optics

A few modifications have been suggested that would make a significant difference to the existing device. The use of two 43mm polarizing lenses is beneficial for the reduction of noise because polarization has been proven advantageous in such configurations, by preventing multiple scattering events from interfering with the resulting data. Another proposed change is the usage of two identical lasers on a beam-merging,

polarizing configuration in order to increase the signal-to-noise ratio of the data. The final proposed change is a three-laser configuration so a dichroic filter could be added to the previously mentioned design along with a waveplate and a laser on a different frequency, allowing the gathering of more information compared to previous designs.[2][3]

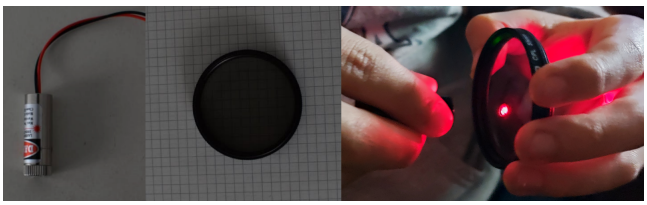

Figure 3: One of the laser diodes (a), a polarizing lens blocking unpolarized light (b), the lens allowing most of the laser diode's light through (c)

IV. Software

The Beaglebone's SoC contains an ARM CPU and two programmable real-time units (PRUs). The ARM processor is responsible for handling the system services of Debian GNU/Linux, such as the handling of sample files, the execution of the main program, the initialisation of the PRUs, and memory management. The PRUs are responsible for driving the photodiode array (PDA) and creating interrupts (PRU0), or for handling the Analog-to-Digital Converter and storing the sensor's data (PRU1). Frame-capturing cycles are divided into three parts, the first of which is integration. During the integration time, the PDA is operated normally but any samples are ignored. Secondly, during the sampling period, the PDA is operated normally and its samples are collected. Lastly, a delaying phase is executed, during which the PRUs do not execute operations, to keep the number of sampling cycles per second equal to the number requested by the user. This process is repeated until the end of the measurement, when the number of recorded frames matches the number requested by the user.[4]

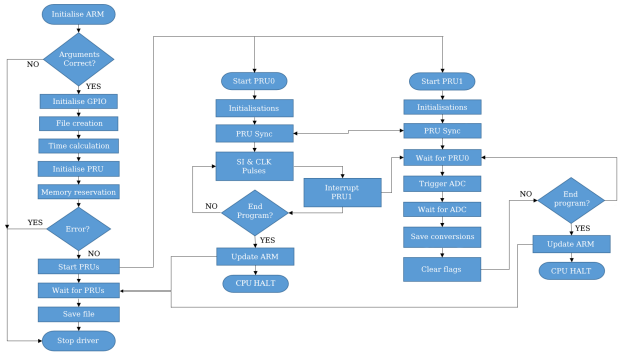

Figure 4: A flow diagram of the software driver[4]

V. Data Analysis & Machine Learning

Since the apparatus currently only records and stores raw data, an external device is required for data analysis. Any personal computer capable of executing C++, Python, and Matlab programs can be used for this purpose. The first programs, developed in Matlab, would execute simple algorithms to determine the accuracy and repeatability of the sensor and would analyse the sample to ascertain the concentration of the particles, the size of the particles, and (for in-vivo samples) the heart rate of the subject. One such program would also draw the Mie plot of the average sample with its expected plot. New programs are currently in development in C++ and Python, implementing more complex algorithms in order to improve the quality of the results and the time efficiency of the process. One such example is programming a good approximation of the model in order to acquire more information about the size, number, and type of particles in the liquid sample.

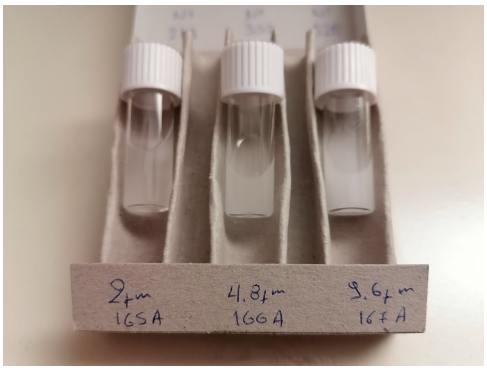

Figure 5: Cuvettes with latex spheres, used for the calibration of the sensor

Assuming a scanning frequency of 50 frames per second and a duration of 5 seconds, the 128-pixel sensor will return a sample of 32000 12-bit unsigned integers every time the code is executed. It is unlikely that a human could adequately recognise patterns between several samples of this size and type. Therefore, machine learning is also being considered as a means to analyse the sensor's data. The training dataset will be *voluntarily* provided by individuals at a microbiological laboratory, where their anonymous samples will be paired with the results of their blood test. A first draft of the multilayer neural network is currently under development in Python. The authors are also looking into unsupervised machine learning algorithms, such as the K-means algorithm, in order to discover any unknown underlying patterns.[5]

References

[1] Karakostas K., *"Portable system development for Mie scattering analysis, to determine the size of blood cells in in-vivo and in-vitro studies"*, Aristotle University of Thessaloniki, 2019

[2] Konstantinos Karakostas, Stratos Gkagkanis, Korina Katsaliaki, Peter Köllensperger, Alkiviadis Hatzopoulos, and Michail E. Kiziroglou, *"Portable optical blood scattering sensor"*, Microelectronic Engineering 217 (2019) 111129, Elsevier

[3] C. Iosifidis, K. Katsaliaki, P. Kollensperger and M. E. Kiziroglou, *"Design of an embedded sensor system for measuring laser scattering on blood cells"*, Bio-MEMS and Medical Microdevices III, SPIE Vol. 10247 102470G-1

[4] Gkagkanis E., *"Fabrication of a photo-diode sensor apparatus with the Beaglebone microcomputer for use in non-invasive biomedical sensors"*, Alexander Technological Educational Institute of Thessaloniki, 2019

[5] Simon Haykin, *"Neural Networks and Learning Machines"*, McMaster University, Hamilton, Ontario, Canada

A Novel Approach on Fault Detection of Analog and Mixed Signal Circuits by monitoring the fluctuation of the Supply Current

V. D. Vassios, A.T. Hatzopoulos and D. K. Papakostas

Department of Information an Electronic Engineering

vassios@el.teithe.gr, ahatz@ihu.gr, dpapakos@ihu.gr

***Abstract*—In this paper, a new method for Fault Detection of analog and mixed signal circuits is presented. The new method is based on measuring the Power Supply Current when the Circuit Under Test is put under a undervoltage stress and monitoring the fluctuation of the power supply current (I_{PS}) to extract new metrics for the normal and faulty behavior of the circuit under test. This method utilizes both Mean and true RMS Current Supply measurements to extract signatures for the under/overshooting of the Power Supply current and the relaxation time that is needed for the circuits to return to their normal, nominal operation. The algorithm for this procedure is presented including preliminary simulation results for the algorithm which is tested on analog circuits.**

***Index Terms*—Analog Circuits, Circuit Under Test (CUT), Fault detection, I_{PS}, Mixed Signal Circuits.**

I. Introduction

Fault detection on analog and mixed signal circuits is an active research field. During the long research over the years, a vast variety of methods and algorithms has been proposed and implemented to detect faults on circuits which appear in the manufacturing process. Using fault detection methods on electronic component/devices, IC manufacturers can enhance the reliability and quality of their products before shipping the products to their customers and speed up the fault diagnosis in components/devices, which leads to a faster repair of the faulty component and ultimately less down time for the device/machine that uses these component/devices [1-4].

The methodology used for the fault detection comprises from a variety of methods/algorithms such as Fault Dictionary Methods [5], Sensitivity Analysis [6], Model Based Analysis [7], Measurement Based Detection [8], I_{PS} measurement [9] and many more. The I_{PS} measurement will be employed for this work and both the Mean and the RMS value of the I_{PS} will be used to extract the good/faulty signature that is needed for the fault detection.

Two approaches are mainly used for creating this signature, the IDDQ (Quiescent Current) [11], where the CUT is not driven by a stimulus signal and the RMS approach where the CUT is driven by an external stimulus signal [12]. By using different metrics such as magnitude/phase [12], spectral analysis [13] wavelet decomposition [14] and a plethora of mathematical tools [15-16] a variety of different signatures can be created.

The classification of the CUTs into good/faulty is achieved with the use of traditional methods such as statistical analysis (standard deviation) [17], topological analysis (Malahanobis distance) [15] or more intelligent approach with the use of neural networks [18] or Support Vector Machines (SVM) [19].

In this work the Under/Over Voltage (UOV) algorithm is presented. This algorithm uses no complex or time-consuming calculations and utilizes the moving average and moving rms algorithm for the extraction of the signature.

II. Abbreviations and Acronyms

NS	Negative Step-Power Supply Transition from 100% to 90%
PS	Positive step-Power Supply Transition from 90% to 100%
$I_{NS}^{min}(rms)$	Minimum rms current value for the negative step transition
$I_{NS}^{rel}(rms)$	Relaxation rms current value for the Negative step transition
$I_{PS}^{max}(rms)$	Maximum rms current value for the Positive step transition
$I_{PS}^{rel}(rms)$	Relaxation rms current value for the Positive step transition
$t_{NS}^{min}(rms)$	Time at which the minimum rms current value for the negative step transition occurs
$tps_{NS}^{rel}(rms)$	Time at which the relaxation rms current value for the Negative step transition occurs
$t_{PS}^{max}(rms)$	Time at which the maximum rms current value for the Positive step transition occurs
$t_{PS}^{rel}(rms)$	Time at which the relaxation rms current value for the Positive step transition occurs
$I_{NS}^{min}(mean)$	Minimum $mean$ current value for the negative step transition
$I_{NS}^{rel}(mean)$	Relaxation $mean$ current value for the Negative step transition

$I_{PS}^{max}(mean)$	Maximum *mean* current value for the Positive step transition
$I_{PS}^{rel}(mean)$	Relaxation *mean* current value for the Positive step transition
$t_{NS}^{min}(mean)$	Time at which the minimum *mean* current value for the negative step transition occurs
$tps_{NS}^{rel}(mean)$	Time at which the relaxation *mean* current value for the Negative step transition occurs
$t_{PS}^{max}(mean)$	Time at which the maximum *mean* current value for the Positive step transition occurs
$t_{PS}^{rel}(mean)$	Time at which the relaxation *mean* current value for the Positive step transition occurs
SPP	Samples per period of the stimulus input signal

III. Review of the Algorithm

The UOV algorithm relies on the fact that all circuits, analog and mixed-signal, will continue to operate properly even if they suffer from a small undervoltage in their voltage supply line. The proposed algorithm measures the time it takes for the circuits to recover and/or stabilize their mode of operation under the new Supply Voltage.

The algorithm comprises of several steps, which are analyzed in greater detail in the next paragraph and summarized below.

Step 1) Wait for the CUT to stabilize in its normal operating mode.

Step 2) The CUT suffers a small under-voltage in its power supply line *(Negative Step)*.

Step 3) The power supply current to the CUT is measured and the mean and rms values are calculated.

Step 4) The minimum value for the current undershooting is measured along with the time it is occurred. $(I_{NS}^{min}(rms), I_{NS}^{rel}(rms), I_{NS}^{min}(mean), I_{NS}^{rel}(mean))$

Step 5) The time it takes for the current to stabilize to its new operating values and these new operating values is measured. $(t_{NS}^{min}(rms), t_{NS}^{rel}(rms), t_{NS}^{min}(mean), t_{NS}^{rel}(mean))$

Step 6) The CUT is driven back to its normal voltage supply values (Positive step).

Step 7) Steps 3 to 5 are repeated one more time for the *Positive Step* and all the corresponding current and time value pairs are calculated. $(I_{PS}^{min}(rms), I_{PS}^{rel}(rms), I_{PS}^{min}(mean), I_{PS}^{rel}(mean))$, $(t_{PS}^{min}(rms), t_{PS}^{rel}(rms), t_{PS}^{min}(mean), t_{PS}^{rel}(mean))$

Step 8) The 8 different current value/time pairs, four the mean values and four for rms values, constitute the signature

Step 9) By repeating step 1 through 8 using Monte Carlo simulation, the variance σ is computed and a detection area of normal current/time values is created which is to be compared against all other CUT measurements.

IV. Detailed Description of the Algorithm

For the testing of the algorithm, a small simple circuit is used. This circuit is a simple CE amplifier depicted in Fig.1.

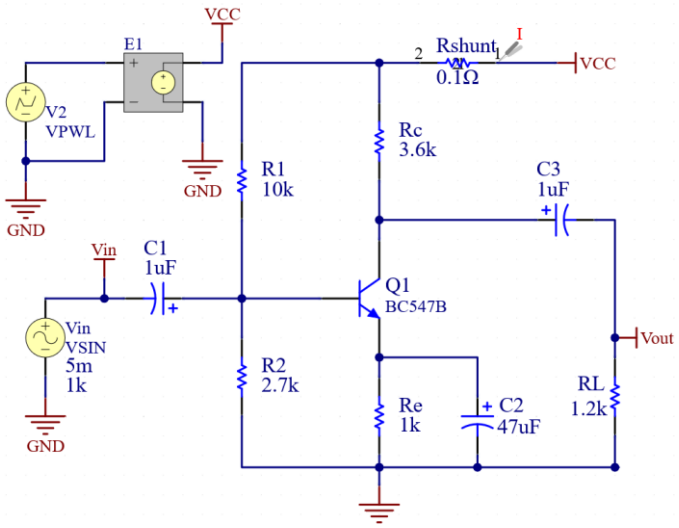

Fig. 1. Schematic description of the CE amplifier.

The circuit is powered from a +12V power supply and stimulated with a 1kHz-10mV$_{(p-p)}$ sinusoidal signal. The Current is sampled at 32kHz. This means that each period of the stimulation signal consists of 32 samples. This value is denoted as Samples Per Period *(SPP)*.

In step 2 the supply voltage drops by 10% from its nominal value, thus driving the circuit to a new state regarding its power consumption i.e., the I_{PS}. In step 6 the voltage supply is returned to its normal operating values. These steps are shown in Fig. 2.

The waveform is separated into two sections. The *Negative Step* (*NS*) and the *Positive Step* (*PS*) denoting the transition from 100% to 90% and from 90% to 100% of the Power supply voltage respectively. The time duration of the Negative step is from the transition from 100%to 90% up to the transition from 90% to 100% and the duration of the positive step is from the transition from 90%to 100% up to the transition from 100% to 90% .These two sections will be processed separately using the same algorithm.

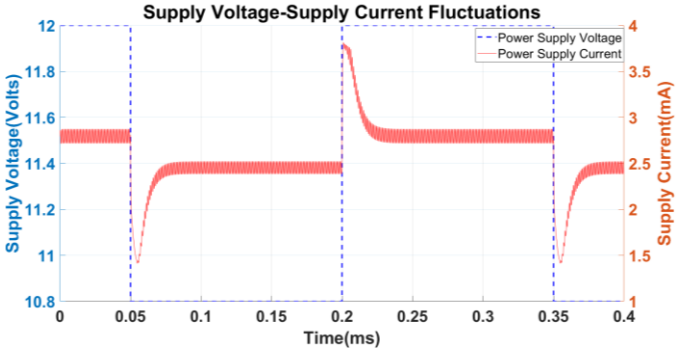

Fig. 2. Time associated Voltage supply and Power Supply Current waveforms

In step 3 the number of samples of both steps are reduced to be proportionate to the SPP, i.e., 32. The mean and the rms values for each step is calculated using the moving(rolling) mean/rms algorithm [20].

For an N-sized sample step with SPP=32 the algorithm that

computes the mean is:

for (k=0 to N-SPP)
do Mean=0, RMS=0
for (i=k+1 to SPP+k)
do Mean=Mean+N(i), RMS=RMS+N^2(i)
do Mean(k)=Mean/SPP, RMS(k)=sqrt (RMS/SPP)

The moving mean and the moving rms calculation decompose the signal shown in Fig 2. to the signals is Fig 3. and Fig 4. which represent the DC and the AC components of the I_{PS} current. Figures 3 and 4 show both Positive and negative step sections of the I_{PS}.

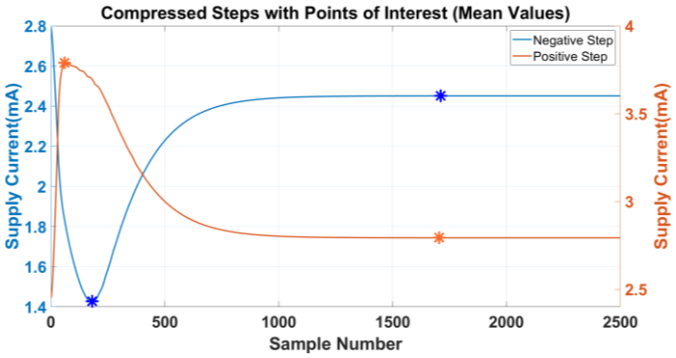

Fig. 3. Mean values (DC component) of the I_{PS} current

In step 4, the current/time pairs for both the maximum values, for the overshooting, and minimum values, for the undershooting, are calculated.

In step 5 the current/time pairs for the settling/stabilization of the I_{PS} are calculated. These calculations use the angle of the slope of the signal to determine the stabilization. This angle is calculated to be 0.15°, which is the angle of charging/discharging slope at time 6τ in a RC charging/discharging circuit.

In step 8, the value of the signature is created by the eight current/time pairs from the mean and rms waveform for both the positive and the negative step.

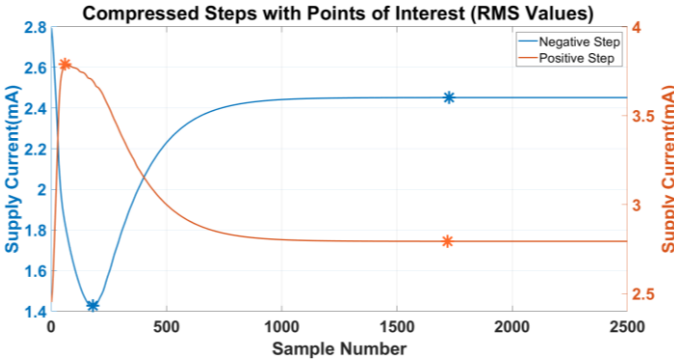

Fig. 4. RMS values (AC component) of the I_{PS} current

In step 9 the Monte Carlo simulation is used to produce new sets of signatures which comprise the set that calculates the standard deviation. For these set of simulations, a standard deviation of 6σ is used. The standard deviation produces an area where all the measurements are considered to belong to a good/working CUT. These areas are shown is Fig. 5 and Fig. 6. Similar signatures with 6σ detection areas are calculated for the positive step also.

The next stage is to inject faults to the CUT and repeat the steps 1 through 8. This will produce a new signature for each fault injected CUT. This signature will be compared against the No-Fault signature by determining if the current/time pairs of the Faulty CUT signature are inside the detection area. For a fault to be detected at least 1 current/time pair must be outside the area of detection. All the No-Fault CUTs must have all 8 current/time pairs inside the area of detection. In any other case the CUT is classified as Faulty.

For the analog Fault modeling, two kinds of faults are introduced to the Circuit Under Test (CUT), Catastrophic(hard) faults and Parametric(soft) Faults. Hard Faults are modeled by inserting ohmic resistances in parallel or in series to all the individual components of the CUT. A resistance of $R_P \leq 1\Omega$ in parallel with any component represents a short circuit to the specific component. On the other hand, a resistance of $R_S \geq 10M\Omega$ represents an open circuit to the specific component. These Hard faults are illustrated in Fig. 5.

Soft or parametric faults are implemented by slightly changing the inherit properties of the components, such as h_{fe}, for the transistors or the W/L values of a MOSFET [10]. After the fault injection the Power Supply Current is measured, and the signature is extracted.

The total number of faults for the CE amplifier are 22, and all the current/time pairs are shown in Fig.6 for the mean and Fig. 7 for the rms values for the *Negative Step* of the I_{PS}.

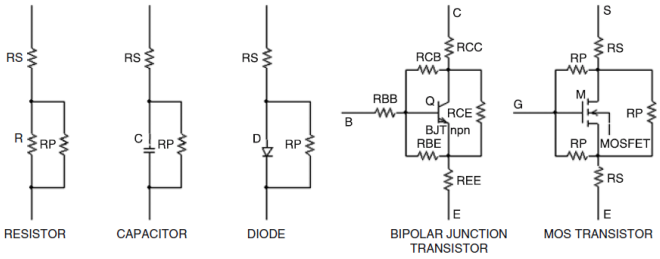

Fig. 5. Fault Modeling on the electronic components in the CUT [10].

The blue dots depict the points of interest for the negative step, i.e., the minimum value for the undershooting of the I_{PS} and the stabilization value of the I_{PS}. The red dots represent the mean value for all the Monte Carlo simulations and the green area shows the deviation (6σ in this set of the simulations) of the Monte Carlo simulations. The asterisks represent the I_{PS} values for the fault injected CUTs.

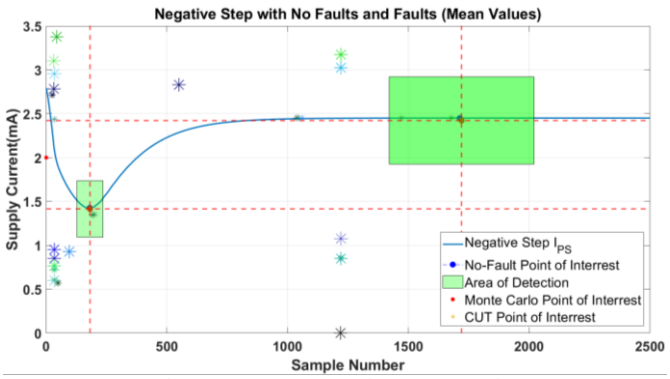

Fig. 6. Scatter plot for the No-Fault/Fault of the CE Amplifier (Mean values).

Similar scatter plots of the No-Fault/Faulty CUT are produced for the positive step also.

The algorithm detected 21 of the 22 hard faults that we were injected into the CUT.

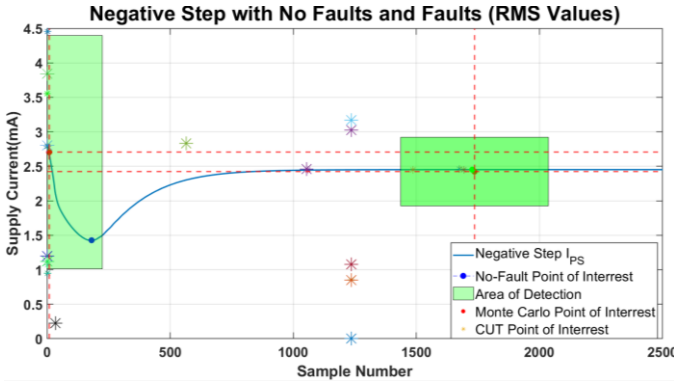

Fig. 7. Scatter plot for the No-Fault/Fault of the CE Amplifier (RMS values).

The algorithm was also applied to a negative feedback amplifier [21], showed in Fig.8, which is a more complicated circuit that has 46 hard faults. The algorithm detected 42 out of 46 hard faults.

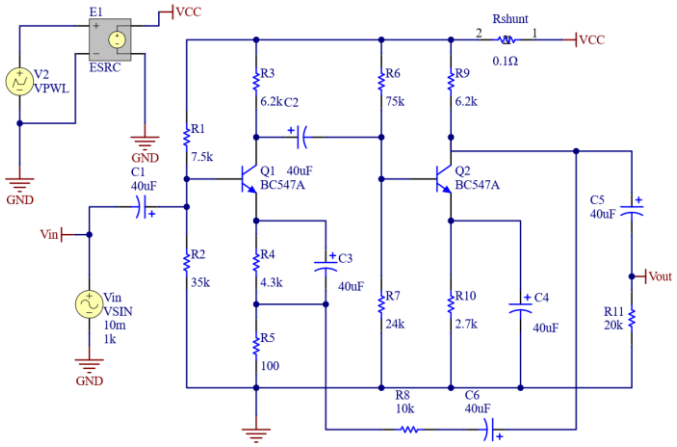

Fig. 8. Negative feedback amplifier [21].

Table I shows the total detectability of the algorithm for the simulations for the two circuits.

TABLE I
FAULT DETECTION RESULTS

Circuit	Number of Faults	Detected Faults	Detectability
Common Emitter Amplifier	22	21	95.45%
Negative Feedback Amplifier	46	42	91.30%

V. CONCLUSIONS AND FUTURE WORK

In this paper a new method for detecting faults in analog and mixed signal is presented. This method utilizes the property of all analog and mixed signal circuits to continue to work properly even if the voltage supply suffers a small, sudden drop in its value. The proposed method measures the under and overshooting values in the power supply current I_{PS} of the CUT, in combination with the settling/stabilization values of the I_{PS} with respect to the time they occur. The algorithm uses the moving mean and moving rms algorithm for the measurement of the I_{PS}. The result produces a much smoother signal which can be processed in finer detail. The algorithm was employed in two circuits. A simple CE amplifier and a two-stage amplifier with negative feedback. The CE amplifier 22 was injected with 22 hard faults and the two-stage negative feedback amplifier with 46 hard faults. The algorithm managed to detect 95.45% of the faults on the CE amplifier and 91,3% of the injected faults for the negative feedback amplifier.

Based on these findings the next step is to apply the algorithm to operational amplifier in all their modes of operations, filters, amplifiers, and comparators. The algorithm at the time is refined to work not only with unipolar circuits but also in bipolar circuits. Also, a PCB with a microcontroller is designed to test the algorithm not only in simulation results, but also with hard data from actual circuits.

REFERENCES

[1] D. Lee, K. Yoo, K. Kim, G. Han, S. Kang,"Code-Width Testing-Based Compact ADC BIST Circuit." IEEE TRANSACTIONS ON CIRCUITS AND SYSTEMS—II: EXPRESS BRIEFS, VOL. 51, NO. 11, NOVEMBER 2004.W.-K. Chen, Linear Networks and Systems. Belmont, CA: Wadsworth, 1993, pp. 123–135.

[2] B.Olleta ,H.Jiang, D.Chen, R.L.Geiger "Methods of testing analog and mixed signal using dynamic element matching for source linearization", US Patent Number:7.587.647B2, September 2009.

[3] M. L. Bushnell, V. D. Agrawal, "Essentials of Electronic Testing for Digital, Memory and Mixed-Signal VLSI Circuits", Kluwer Academic Publishers,2000.

[4] M. Burns and G.W. Roberts, An Introduction to Mixed-Signal IC Test and Measurements, Oxford University Press, New York, 2001.

[5] Bandler John W, Salama Aly E. Fault diagnosis of analog circuits. In: Proceedings of IEEE, vol. 73, 8;1985. p. 1278–1325.

[6] Milne A, Taylor D, Naylor K, Assessing and comparing fault coverage when testing analogue circuits. In: Proceedings of IEEE conference on circuit devices and systems, vol. 144, 1; 1997. p. 1–4.

[7] Catelani M, Giraldi S. Fault diagnosis of analog circuits with model-based technique. In: Proceedings of IEE conference on instrumentation and measurement; 1998. p. 501–4.J.

[8] Rodríguez-Blanco Marco Antonio, Claudio-Sánchez Abraham, Theilliol Didier,Vela-Valdés Luis Gerardo, Sibaja-Terán Pedro, Hernández-González Leobardo,Aguayo-Alquicira Jesus. A failure-detection strategy for IGBT based on gate-voltage behavior applied to a motor drive system. IEEE Trans Ind Electron 2011;58(5):1625–33.

[9] D.K. Papakostas and A.A. Hatzopoulos, "Supply current testing in linear bipolar ICs", Electronics Letters, pp. 128-130, January 1994.

[10] R. Kondgunturi, E. Bradley, K. Maggard, C. Stroud "Benchmark circuits for analog and mixed-signal testing.", Conference Proceedings IEEE SOUTHEASTCON (1999) 1999-March 217-220

[11] T. A. Unni and D. M. H. Walker, "Model-based IDDQ pass/fail limit setting," in Proc. of IEEE Int'l Workshop on IDDQ Testing, pp. 43–47, Nov. 1998.

[12] D. K. Papakostas, A.A. Hatzopoulos, "A Unified Procedure for Fault Detection of Analog and Mixed-Mode Circuits Using Magnitude and Phase Components of the Power Supply Current Spectrum", IEEE Trans. Instrument. Meas., vol. 57, No. 11, November 2008.

[13] A.A. Hatzopoulos, "Analog Circuit Testing", Proceedings of the 2017 IEEE 22nd International Mixed-Signals Test Workshop, IMSTW 2017.

[14] A D. Spyronasios, M G. Dimopoulos, A. A. Hatzopoulos, "Wavelet Analysis for the Detection of Parametric and Catastrophic Faults in Mixed-Signal Circuits", ", IEEE Transactions on instrumentation and measurement, vol. 60, No. 6, July 2011.

[15] M.F Toner, G.W. Roberts, "A BIST scheme for an SNR test of a sigma-delta ADC," IEEE Int. Proc. Test. Conference 1993.

[16] K. Wang*, Y. Guana, D. Lib, X. Lic, J. Guand,"Research on Fault Diagnosis of Analog Circuit Based on Volterra Theory and Higher-Order Spectrum Analysis", IOP Conf. Series: Materials Science and Engineering 782 (2020) 032096.

[17] W. Hochwald and J.D. Bastian, "A dc approach for analog fault dictionary determination", *IEEE Transactions on Circuits and systems*, Vol. CAS-26, pp. 523-529, July 1979.

[18] C. T. Chen ,C. T. Yen, C. H. Wen, C. Y. Yang, C. H. Wu, K. C. Chern, M. Chen, Y. Y. Kuo, C. Y. Lee, J. N. Kao, S. Yi, "CNN-based Stochastic Regression for IDDQ Outlier Identification", Proceedings of the IEEE VLSI Test Symposium, Vol: April 2020.

[19] Z. Zhang, Z. Duan, Y. Long, L. Yuan, "A new swarm-SVM-based fault diagnosis approach for switched current circuit by using kurtosis and entropy as a preprocessor", Analog Integrated Circuits and Signal Processing, Vol:81, pp.289-297, August 2014.

[20] Η. Λιώκη-Λειβαδά, Δ. Ασημακόπουλος, "Μαθήματα εφαρμοσμένης στατιστικής",1st ed. Athens, Greece, Εκδόσεις Συμμετρία, pp. 481-485.

[21] Y. Deng, G. Chai," Soft Fault Feature Extraction in Nonlinear Analog Circuit Fault Diagnosis", Circuits, Systems, and Signal Processing, vol 35, No. 12, pp. 4220-4248,2016

Rectification and boosting circuit for acoustic power transfer

Vasileios Fountas(1)*, Dimitrios Makarikas(2), Michail E. Kiziroglou(2), Konstantinos Karakostas(3) and Alkiviadis Chatzopoulos(1)

(1) Department of Electrical and Computer Engineering, Aristotle University of Thessaloniki
(2) Department of Industrial Engineering and Management, International Hellenic University
(3) Department of Electronics, Echovista GmbH, United Kingdom

***Abstract*— The purpose of the system is to harness the energy generated by piezoelectric acoustic receivers and maximize it through by an impedance matching rectification circuit. A sound wave carries acoustic energy and its mechanical energy can generates voltage on a piezoelectric element. We use a supercapacitor or a battery to store the electrical energy of the system. The energy harvesting power management system includes certain building blocks to ensure maximum transferred power. First, it requires the conversion of AC to DC through a rectifier. The use of a DC-to-DC converter is necessary to increase the voltage to the desirable supercapacitor storage and load level. To implement the boosting, storage control and regulation functions, a commercial integrated circuit is employed which complies with the appropriate requirements for the system characteristics. In this paper a complete acoustic power transfer architecture, including a power management circuit with a custom active rectifier, is presented. The circuit design is discussed and preliminary transducer-level experimental results from acoustic power transfer through a planar metal structure are presented.**

***Index Terms*—Thermoelectric energy harvesting, impedance matching, power management, active rectification**

I. INTRODUCTION

Acoustic power transfer

Acoustic energy can penetrate through solids, liquids and gases and can be produced from any kind of mechanical vibrations. The propagation of the acoustic wave away from the source at a finite speed is a function of the elastic properties and density of the medium, and is governed by the wave equation. The applications on the field of energy harvesting have increased including TEG, piezoelectric and solar circuits. Referring to acoustic power transfer applications, the problem to be solved is the demand of solid structures with standard geometry. Otherwise, the efficiency is reduced and the transmitter cannot maximize the power that could be propagated to the receiver through acoustic waves. The amount of power transferred and the efficiency depend on the source and load impedances, as well as on the source power. In addition, the piezoelectric is a resonant system. It produces maximum output power when excited at its resonance frequency. Therefore, resonant frequency tuning is the technique used in such an application, so as to avoid reflection of the sound waves leading to a reduction in the output power of the piezoelectric element.

Impedance matching

Any electrical device which demands a signal for its operation has an input impedance. The measurement of the input impedance could be done with an oscilloscope or with an AC voltmeter. On the other hand, the output of a system can be modeled as a voltage or current generator in combination with an output impedance Z_{OUT}. Taking a voltage model as an example, if the output terminals are loaded by a resistor, or by the input terminals of another circuit, part of the voltage generator open-circuit output voltage V will be lost on Z_{OUT}.

In a simple circuit, the maximum power transfer theorem demands that in order to transfer the maximum power from the source to the load, the load impedance must be equal to the complex conjugate of the source impedance: $Z_{LOAD} = Z_{OUT}^{*}$. The problem of mismatched impedances of source and load could be solved in order to optimize power transfer by connecting a circuit between them. Such circuits are called impedance matching circuits and their design is not always simple. Piezoelectric acoustic receivers usually have a capacitive output impedance, and therefore it can be compensated by adding an inductor as an impedance matching circuit between the piezoelectric and the load.

The description of our system which is shown on *Fig.1* refers to acoustic power transfer, so the examination of acoustic impedance matching is also needed. The addition of single matching layers or multiple matching layers offers several different acoustic impedance matching techniques. The single layer one is less complex than the multiple layer one, since only a layer is needed between the medium and the transducer. The disadvantage comparing to multiple matching is that a range of variable frequencies is not available. Also, the thickness of the layer is often set to a quarter of the wavelength (where $c = \lambda f$). The interface impedance is then equal to the square root of the product of the transducer and the medium impedances.

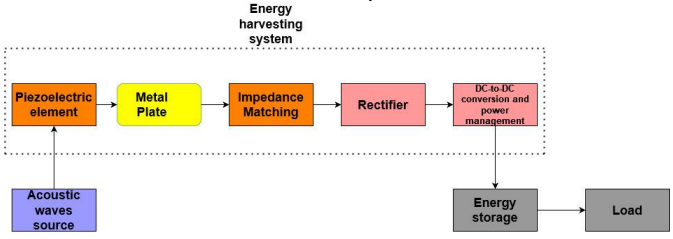

Fig. 1: Block Diagram of our system

II. ACTIVE RECTIFICATION

A schematic of the active rectifier is shown on *Fig 2*. It follows the rectification architecture proposed in [1]. It consists of eight Infineon BSP149 n-channel depletion MOSFETs and two Vishay SQD100N03-3m5L n-enhancement MOSFETs, one low-power comparator MAX9120EXK+T and a MAX1721EUT+T switched-capacitor voltage inerter both from Maxim. The choice of the n-channel depletion MOSFETs was based on the low R_{ds} and Vth. Due to their relatively high $R_{DS,ON}$, four depletion MOSFETs were connected in parallel for each branch of the bridge. The n-channel enhancement MOSFETs were also chosen based on their low $R_{DS,ON}$ but the values available on the market were adequately low and therefore the connection of multiple components in parallel was not necessary. More specifically, the n-channel depletion MOSFETs have typical values of V_{th}=-1.4V and R_{ds}=1.7Ω. The n-channel enhancement MOSFETs have typical values of V_{th}=2V and R_{ds}=0.0030 Ω. The comparator detects the polarity of the piezoelectric voltage and produce gate signals for the enhancement MOSFETs. The input signal of the voltage inverter is also generated from the comparator and controls the n-depletion MOSFETs. On *Fig.2*, the piezoelectric receiver is modeled by an AC voltage source.

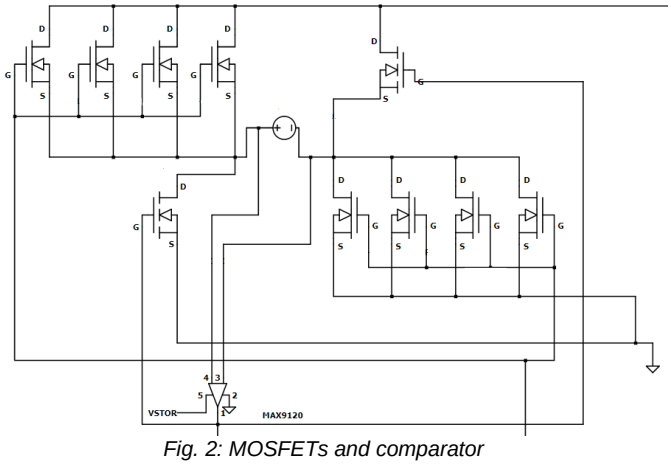

Fig. 2: MOSFETs and comparator

To drive the depletion MOSFET gates with the required negative bias, an inverter is used to invert the voltage applied to the circuit. The inverter circuit is shown in *Fig. 3*. The flying capacitor (C1) has a relatively low value, because the increase of it will cause the increase of the output resistance. Also, increasing the value of the output capacitor (C2) will cause the reduction of the output ripple voltage. As shown on *Fig. 3*, the V_{out} pin of the inverter is connected to the junction where the gate signals of the n-depletion MOSFETs are connected. The V_{in} pin is connected to the $\overline{SHDN}$ pin and the junction of the them is connected to the junction of the comparator output and the connection of n-enhancement MOSFETs gate signals.

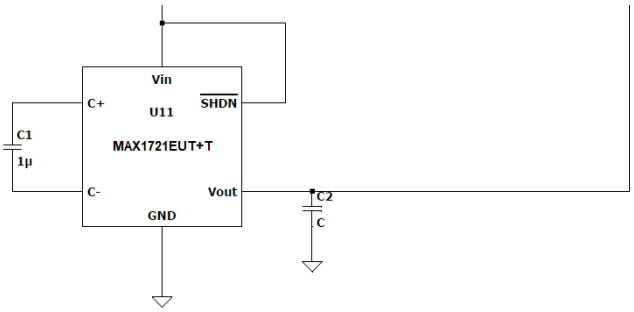

Fig. 3: Voltage Inverter

III. POWER MANAGEMENT AND HARVESTING CHIP

On *Fig.4* we follow the connections of the typical piezoelectric energy harvesting application for the BQ25570 chip [5]. This module is used to finally charge a supercapacitor. To calculate each resistance we used the formulas used in the datasheet of the IC, which is quite important since they form a voltage divider. In this project we also use an SSQ-108-23-G-D female header with 16 positions, to allow access to various pins for testing and performance characterization. All the capacitors need to be low leakage, because that will reduce the efficiency of the energy harvesting. Also, in our application we are choosing the minimum CSTOR capacitance which is 4.7uF. If our storage element has higher impedance than the expected, we need to either increase this capacitance or add capacitance to VBAT pin to maintain a fast VSTOR charge. The VSTOR pin is very important, since is it is used to supply the comparator used in the rectifier.

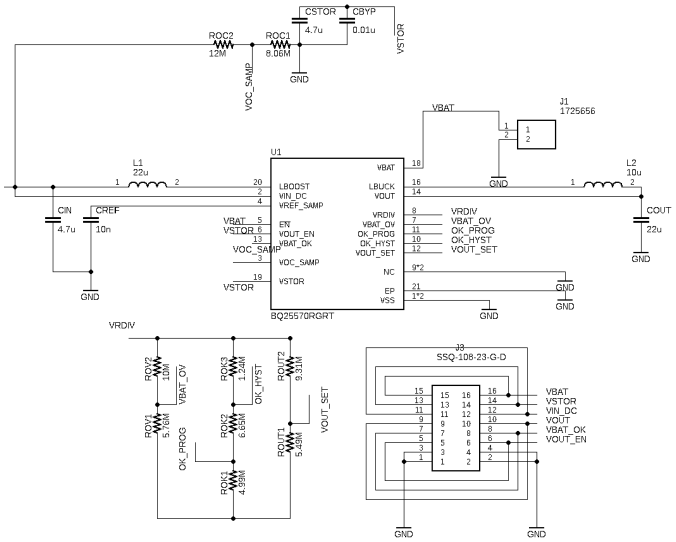

Fig. 4: BQ25570 chip, pin connections and pin headers for external measurements.

The use of the VSTOR instead of a battery is necessary for our energy harvesting system. The selection of the boost charger and buck converter inductors is based on the normal control of their switching behavior.

Furthermore, the resistance values of the voltage dividers of the BQ25570 chip are specified to set the following voltage threshold values: The battery overvoltage protection is set to VBAT_OV = 5 V (;). The battery OK indicator threshold is set to VBAT_OK_HYST = 3.1 V for increasing voltage and to VBAT_OK = 2.8 V for decreasing voltage. The regulated output voltage is set to VOUT = 3,3 V . Using the appropriate equations we calculate the resistance value for the above thresholds.

IV. PCB LAYOUT

The layout of our PCB is being constructed based on several design and fabrication rules that we adopted. The ground plane is used in bottom layer only.

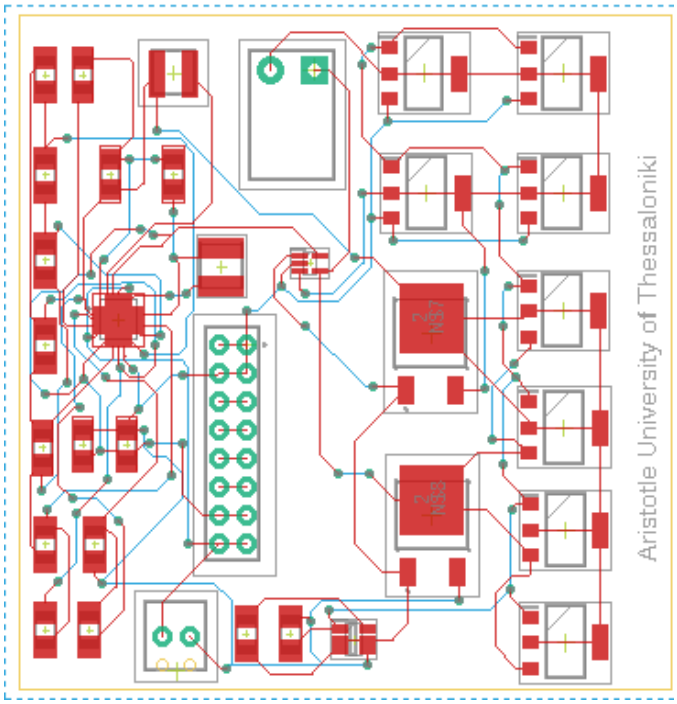

Fig. 5: Layout designed on Autodesk Eagle

Since we are using full wave rectification, it is demanded that we gather both the depletion and the enhancement MOSFETs on the same side. For the better connections concerning the BQ25570 chip, we selected the best paths to avoid the construction of extra vias. The vias have a drill of 0.35mm and the wires of the top and bottom side have a width of 6. The dimensions of the PCB are 60 mm × 60 mm. The capacitor and resistor packages were chosen to be C1206 and R1206 respectively. Also, through hole connectors were selected instead of SMD ones to allow faster and more practical laboratory testing. A silk layer is used to name our PCB. At this point we can refer to the fact that the low voltage outputs on our design allow us to use wires with less width. The more width we use on our wires, the more current can be carried.

V. EXPERIMENTAL RESULTS

The experiments that are being presented on this paper include the results from an energy harvesting layout. A vibration speaker element was chosen as an acoustic wave source, attached to one side of an 1000 mm × 500 mm × 3 mm aluminum plate. A signal generator in combination with a customized audio amplifier was used to drive the speaker transducer. The generator is necessary to test how the output voltage changes when different frequencies are being applied. A 20 mm diameter piezoelectric diaphragm with 300 Ω resistance, 45 nF capacitance and 2000 Hz resonance frequency (all nominal values) was used as the receiver. The experimental setup is shown in Fig 6.

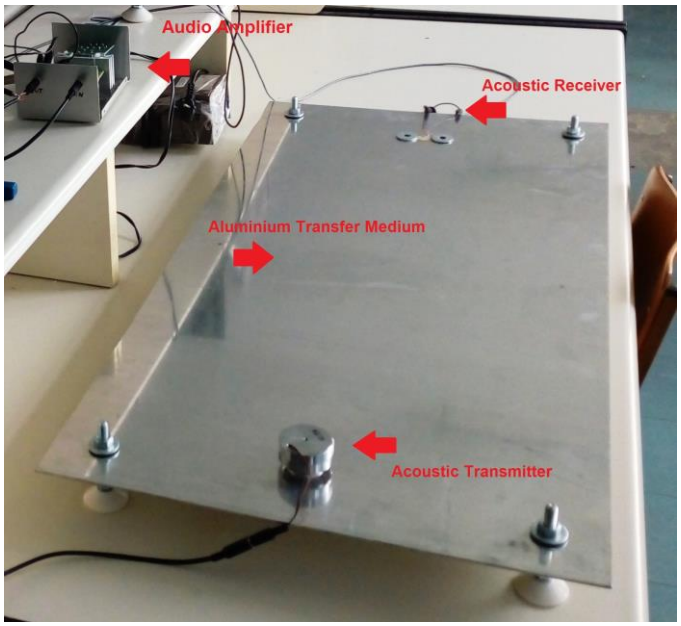

Fig. 6: Acoustic waves source located distantly from the piezoelectric element on a metal plate

In the experiments signals in the acoustic frequency band were tested, i.e. between 20 Hz and 20 kHz. Simultaneous measurements of voltage on the transmitter and the receiver were performed in order to include the phase difference in the characterization.

The distance and the position of the source on the metal plate is quite important, since the generated power differs while testing the output values on different frequencies. Measurements at different distances were performed. Indicative results at a transmitter – receiver distance of 800 mm for various frequencies are shown in Fig. 7. The received power was measured on a matched resistive load without reactance cancellation. The effect of standing wave phase difference is observed. The standing wave maximum power positions shift with the applied frequency, resulting in power oscillation with frequency at the stationary receiver location.

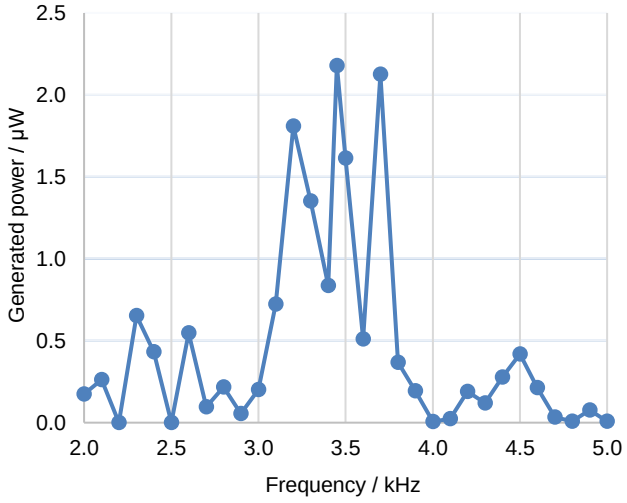

Fig. 7: Active power / Frequency

The scaling of received power with increasing transmitted power was also studied. Experimental measurements for transmitted average power up to 5 W are shown in Fig. 8. The transmitter power was measured as the real average electrical power $P = IVcos\varphi$ on the speaker, where I, V and φ are the RMS current, RMS voltage and I-V phase difference respectively. The measurement of current was performed by an oscillator channel connected across a 0.1 Ohm resistor which was added to the circuit in series with the speaker, for this purpose. Received power as high as 1.6 mW is demonstrated corresponding to a power transfer efficiency of 0.027 %. The maximum demonstrated efficiency is observed at 0.33 W transmitter power, yielding a received power of 0.18 mW and a transfer efficiency of 0.056%.

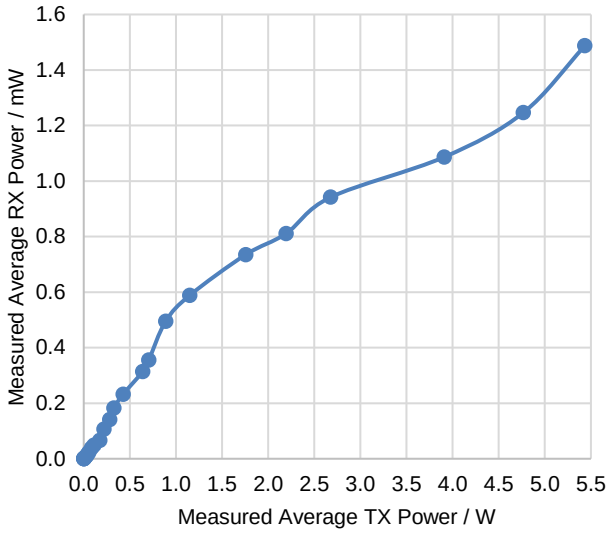

Fig. 8: Generated power/ transmitter power

VI. SUMMARY

An acoustic power transfer system through metal structures is proposed. A power management system is designed, identifying efficient rectification and complex impedance matching as key parameters to performance improvement. An experimental setup for acoustic power transfer through a 3 mm thick aluminum plate was developed, demonstrating a power transfer of 1.6 mW at a distance of 800 mm from a 5.5 W speaker, using a 314 mm^2 area receiver.

One of our goals is to increase the received power by complex impedance matching. The implementation and testing of the power management system in the developed acoustic power transfer setup is expected to increase the received power and offer a regulated power source for distributed wireless infrastructure sensors.

REFERENCES

[1] T. Toh, S.W. Wright, M.E. Kiziroglou, P.D. Mitcheson, E.M. Yeatman, “A dual polarity, cold-starting interface circuit for heat storage energy harvesters”, Department of Electrical and Electronic Engineering, Imperial College London, London SW7 2AZ, UK, 2014.

[2] M.E. Kiziroglou , D.E. Boyle, S.W. Wright, E.M. Yeatman, “Acoustic power delivery to pipeline monitoring wireless sensors”, Department of Electrical and Electronic Engineering, Imperial College London, London SW7 2AZ, United Kingdom, 2017

[3] Hamid Basaeri, David B Christensen and Shad Roundy, “A review of acoustic power transfer for biomedical implants “, Department of Mechanical Engineering, University of Utah, Salt Lake City, UT, USA, 2016

[4] O Freychet , F Frassati, S Boisseau , N Garraud , P Gasnier and G Despesse, “ Analytical optimization of piezoelectric acoustic power transfer systems “, Univ. Grenoble Alpes, CEA, Leti, F-38000 Grenoble, France, 2020

[5] Vivek T. Rathod, “A Review of Electric Impedance Matching Techniques for Piezoelectric Sensors, Actuators and Transducers “, Department of Electrical and Computer Engineering, Michigan State University, East Lansing, MI 48824, USA, 2019

[6] Briand D, Yeatman E and Roundy S (ed) 2015 Micro Energy Harvesting (Weinheim: Wiley)

[7] Nakamura K 2012 Ultrasonic Transducers: Materials and Design for Sensors, Actuators and Medical Applications (Amsterdam: Elsevier)

[8] Zaid T, Saat S, Yusop Y and Jamal N 2014 Contactless energy transfer using acoustic approach—a review 2014 Int. Conf. on. IEEE Computer, Communications, and Control Technology (I4CT) (doi:10.1109/I4CT.2014.6914209)

[9] Ozeri S and Shmilovitz D 2010 Ultrasonic transcutaneous energy transfer for powering implanted devices Ultrasonics 50 556–66

Automation of a Washing Machine: An Open-Source Approach

K. Kostopoulos+, D. Triantafyllidis
International Hellenic University / Department of Industrial Engineering & Management
P.O. Box 141, 57 400 Sindos, Thessaloniki, Greece

+ Corresponding author: kostas.kh@gmail.com

***Abstract* — Many modern washing machines reach their end of life prematurely due to failure of the electronics, while the mechanical part is still in perfect order. The present work aims to automate and revive a washing machine using freely available low-cost hardware. An Arduino microcomputer was programmed to replace the build-in central control unit. The Proteus Design Suite program was used for code testing and system simulations. During the project, the operations of the components and the basic washing programs of a real washing machine were studied in order to write the code. A driving system for the washing machine's motor was also designed to properly accommodate each washing program. All the above provide a system that offers the main operations of a modern washing machine.**

Keywords* — *Washing Machine, Arduino, Proteus Design Suite

I.INTRODUCTION

The washing machine is an integral part of the modern household. Unfortunately, sometimes failure of the electronic components of the unit, lead to expensive repairs, which make it more preferable to replace the whole washing machine, than to repair it. This does not only have an economic impact, but furthermore adds to the ecological problems the planet faces these days. The present work has been conducted to examine the washing machine's automation and face the issue using an open-source approach to the above problem. The primary goal was to use a microcomputer to replace the faulty central control unit (mainboard) of a real washing machine. However, because of the unprecedented situation of the Covid-19 pandemic, the project was simulated with the Proteus Design Suite, which was assessed as an appropriate software for the simulation [1].

The washing machine control system has been divided into lower voltage and higher voltage. In the lower voltage category, components work at DC +12V, such as the water temperature sensor, the water level sensor, pushbuttons, the door locks sensor, the buzzer and an I2C liquid crystal display. In the higher voltage category, there are components that work with AC 230V. Those components are the water heater, the valves and the pump. In order to control these items, relays must be used to isolate lower voltage from higher voltage systems [2].

II. THEORETICAL FRAMEWORK

The washing machine parts have been divided into two main categories. The first category is related to mechanical parts such as the drum with two tubs and the agitator fins—the former consists of the inner and outer tub. The clothes are placed into the inner tub, which is surrounded by holes in order to allow the water to move in and out. The outer tub contains the inner tub and the water. The next part is the detergent container. In most cases, it will have up to four departments for the detergent, the softener and pre-wash. Additional parts include two hoses, one being responsible for the clean incoming water and the other for the outgoing dirty water. In addition, a washing machine has a glass door, which is locked during washing. One more mechanical part is the filter, which is located at the machine's bottom. The filter's functionality is to trap anything from lint to hair and keep the laundry machine clean and protect the pump.

The second category is related to electrical parts. The central part is the mainboard, where all the other electrical parts are connected. The mainboard has to switch the electrical parts on or off according to a time schedule or sensor inputs. This system can be called an input-output system. The input system refers to the sensors and the pushbuttons powered by 12V DC, and the output refers to the valves, the pump, the motor, the buzzer, and the thermal element. At present, washing machines will have at least three sensors. The most common sensors are responsible for the temperature (Negative Temperature Coefficient, NTC) [3] and the level of the water (Pressure Switch). Finally, the last is a speed sensor mounted on the motor shaft. Manufacturers use valves to control the incoming water for different parts in the washing machine, such as the water in the drum and the water in the detergent container. In addition, they use the pump to promote the dirty water through the hose to the drainage system. The next part is the motor, which in most cases is a universal type brushed motor [4]. The motor transfers movement to the drum, via a belt. One more output part is the heating element, located in the same place as the temperature sensor, in the downside of the drum. Typically, the heating element is 1900-2200 W. The last part of the output system is the door lock system. Usually, it is an electromagnetic or a bimetallic lock. The utility of this part is to keep the door locked until the washing cycle ends.

III. HARDWARE DESIGN

The hypothesis of the project is that the mainboard has been damaged and all the other components are in good working order. To replace the mainboard an Arduino UNO R3 microcomputer has been used. Because the Arduino UNO can handle only DC voltage, it has to be connected with the AC parts via relays to isolate the two electrical systems. Next, a driving system for the motor was designed using a single-phase bridge rectifier and an H-bridge with four MOSFETs. The driving system has been connected to the Arduino through two MOSFET drivers, by using two digital pins in PWM mode. After that, the washing machine's sensors are being connected to the Arduino's analogue inputs so that the microcontroller can read their values. Finally, pushbuttons have been connected to Arduino's digital pins.

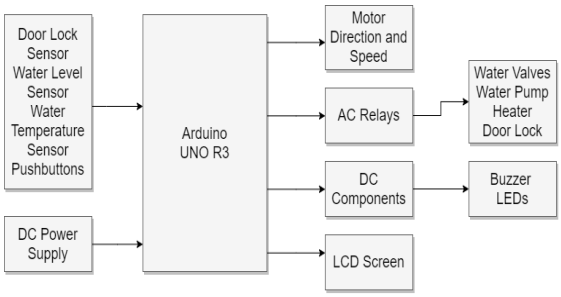

Fig. 1. Block Diagram of Microcomputer for Washing Machine.

Due to the problematic situation with the Covid-19 pandemic, the whole project was simulated with the Proteus Design Suite (PDS). This environment has almost all the needed components, and it can simulate the project almost as if in the real world. From the PDS library the Arduino UNO R3, four pushbuttons, a buzzer, and five led lights to simulate the pump, the valves and the door lock were chosen. Two virtual potentiometers were added to simulate the water level and water temperature in place of real sensors. Additional parts necessary include the LCD screen with the I2C protocol [5], the motor and the motor driver with the MOSFETs and MOSFET drivers.

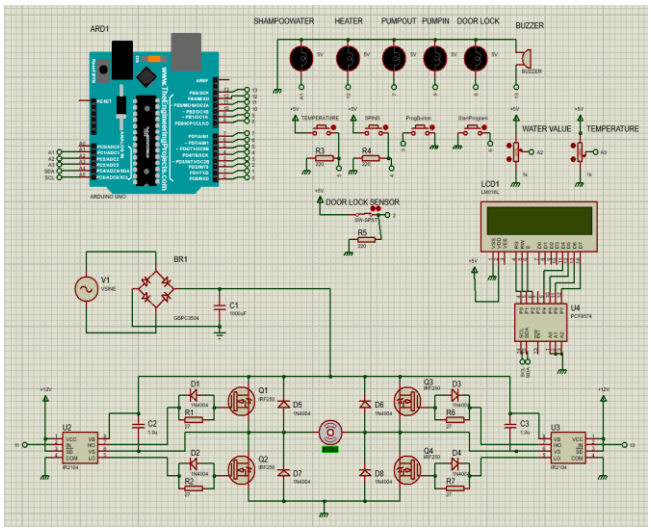

Fig. 2. Schematic of washing machine in Proteus Design Suite.

Each component's terminal must be connected to the correct pin on the Arduino so that the system works, according to Table I.

TABLE I: ARDUINO PINS

Arduino Pin	Input/Output	Description
2	Input	Door Lock Sensor
3	Input	Pushbutton Programs
4	Input	Pushbutton Spins
5	Input	Pushbutton Temp
6	Input	Pushbutton Start
7	Output	Pump Water
8	Output	Lock Door
9	Output	Valve Water
10	Output	Motor1 (PWM)
11	Output	Motor2 (PWM)
12	Output	Heater
13	Output	Buzzer
A1	Output	Valve Shapoowater
A2	Input	Water Level
A3	Input	Water Temperature
A4	Output	LCD (I2C)
A5	Output	LCD (I2C)

IV. SOFTWARE DESIGN CRITERIA

The software should meet at least the following design criteria for the requirements of a typical, commercially available, washing machine [6]:

- Lock the door for safety.
- The inner tub should be able to move in two directions and at a specified range of speeds during various phases of the washing program.
- The water should be heated and controlled.
- The water level should be controlled.

V. SOFTWARE DESIGN

The required software for the project has been created using the Arduino IDE. It includes eight different washing programs, of which one is for testing purposes, and the others are for actually washing the clothes.

TABLE II: WASHING PROGRAMS

#	Name of function	Washing Programm	Duration (min)
1	cottons()	Cotton	202
2	white()	White	162
3	quickwash()	Quick Wash	30
4	wool()	Wool	45
5	ecomode()	ECO mode	237
6	sensitive()	Sensitive	62
7	spin()	Spin	10
8	test()	Test for simulation	5

The code includes functions to check the sensors and turn on or off the required components to create a fully working washing machine. Additionally the code controls the washing machine's human machine interface (buzzer and LCD screen) and the motor's direction and speed.

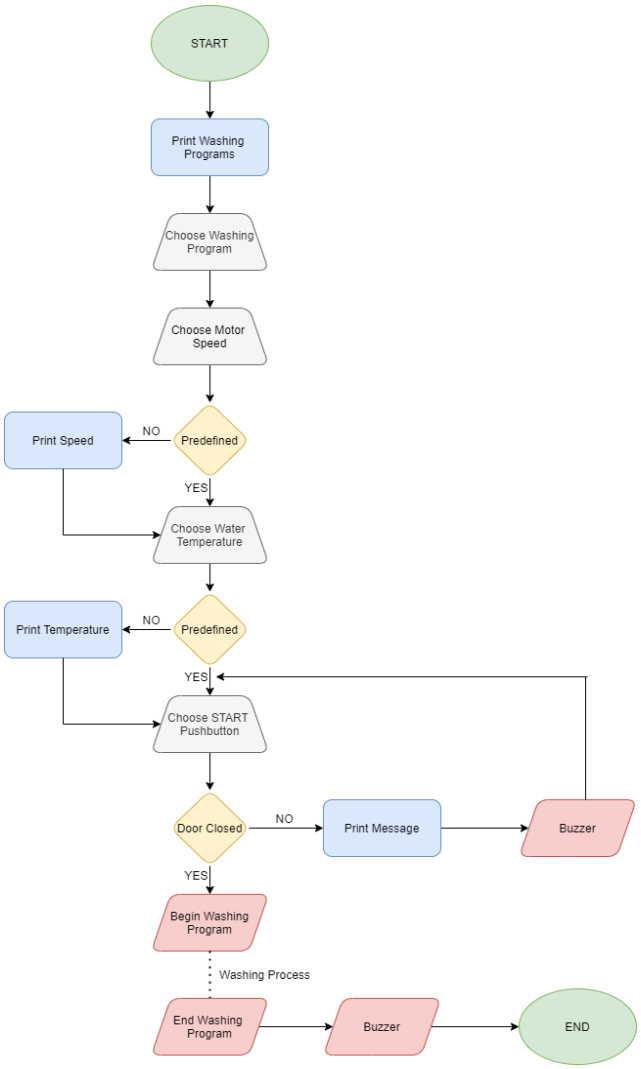

Fig. 3. Flow Chart for Main Process of Washing Machine.

VI. CONCLUSIONS AND FUTURE WORK

The solution is completely custom engineered for the needs of the proposed application. The design is promising and can be applied to the majority of washing machines. Moreover, it can be customized and optimized via the Arduino IDE to add more washing programs. In terms of cost it is a cost-effective solution since the price of the Arduino microcomputer is very low compared to a new mainboard.

Future work will allow adding more functionality easily to keep the washing machine up to date and valuable, such as remote control and notifications to smartphones. Finally, future work should include the actual implementation of the proposed project with real hardware, which will additionally require a closed-loop feedback control of the motor speed, not implemented in this simulation.

REFERENCES

[1] Labcenter. PCB Design & Simulation Made Easy. Available from: https://www.labcenter.com/.
[2] Manurung, M., et al., “Door Security Design Using Fingerprint and Buzzer Alarm Based on Arduino: English.” Journal of Computer Networks, Architecture, and High-Performance Computing, vol. 3, p. 42-51, 2021.
[3] Fraden, J., “Handbook of modern sensors: Physics, designs, and applications,” 2003.
[4] Chapman, Stephen J., “Electric Machinery Fundamentals,” 5th ed. 2019.
[5] Akinwole, O. and T. Oladimeji, “Design and Implementation of Arduino Microcontroller Based Automatic Lighting Control with I2C LCD Display,” Journal of Electrical & Electronic Systems, 2018.
[6] Whirlpool, Service Manual.